Physica B 593 (2020) 412243

Contents lists available at ScienceDirect

Physica B: Physics of Condensed Matter

journal homepage: http://www.elsevier.com/locate/physb

Effective partition function of crystals: Reconstruction from heat capacity data and Debye-Waller factor

Roman Tomaschitz

Sechsschimmelgasse 1/21-22, A-1090, Vienna, Austria

ARTICLE INFO

Keywords:
Varying Debye temperature
Temperature-dependent spectral cutoff
Zero-point energy
Internal energy and entropy
Debye-Waller *B*-factor
Rutile polymorph of titanium dioxide

ABSTRACT

A semi-empirical method to define a partition function for phonons is proposed, which is capable of accurately reproducing thermodynamic functions, especially in the intermediate temperature range, where the Debye theory occasionally fails to describe the emerging phonon peaks in the heat capacity. The phonon partition function is defined with a temperature-dependent spectral cutoff $\Lambda(T)$ and Debye temperature $\theta(T)$. The varying $\theta(T)$ can be reconstructed from heat capacity measurements by least-squares regression, and the spectral cutoff is chosen so that the partition function defines a genuine equilibrium system consistent with the equilibrium condition $\partial S/\partial U = 1/T$ on the internal-energy derivative of entropy. The zero-point energy of the phonons is not predetermined by the amplitude of the cubic low-temperature slope of the heat capacity but emerges as an integration constant, which can be inferred from X-ray diffraction measurements of the Debye-Waller *B*-factor. The formalism is put to test with the rutile polymorph of TiO_2.

1. Introduction

The purpose of this paper is to find an effective partition function for crystals that can be used to accurately reproduce measured heat capacity data, especially the crossover from the cubic temperature dependence of the lattice heat capacity to the high-temperature regime, which is not always accurately reproduced by the standard Debye theory of heat capacity. One frequently employed method to model this crossover, especially in experimental papers [1–6], is to assume a temperature-dependent Debye temperature $\theta(T)$ to be determined by a fit of the heat capacity to the measured data points, after conversion from isobaric to isochoric heat capacities. However, a phonon partition function with varying Debye temperature does not any more define an equilibrium system. In particular, the equilibrium condition $\partial S/\partial U = 1/T$ on the internal-energy derivative of entropy is violated once the Debye temperature becomes temperature dependent. Here, we show how to preserve this relation by allowing the spectral cutoff $\Lambda(T)$ of the partition function to also vary with temperature, in addition to $\theta(T)$. The cutoff $\Lambda(T)$ can be related to $\theta(T)$ so that the equilibrium condition $S_{,U} = 1/T$ is satisfied. Both functions $\Lambda(T)$ and $\theta(T)$ can be determined from a fit of the isochoric heat capacity to the data sets.

Another distinct difference to the Debye theory with constant Debye temperature and frequency cutoff is the zero-point energy of the phonons, which is not defined by the constant Debye temperature but is a free integration constant. This integration constant, which also affects $\Lambda(T)$ and $\theta(T)$, can be determined by measuring the Debye-Waller factor $B(T)$ via X-ray diffraction. In contrast, in the Debye theory, $B(T)$ is already determined by the constant Debye temperature (inferred from the amplitude of the low-temperature T^3 slope) and usually differs noticeably from the measured values.

Starting with the partition function of the standard Debye theory, we develop the thermodynamic equilibrium formalism adapted to a varying Debye temperature $\theta(T)$ and spectral cutoff $\Lambda(T)$ and put it to test by applying it to heat capacity data sets of rutile titanium dioxide. Heat capacity data are available for the rutile polymorph continuously from the low-temperature regime up to the melting point, and the Debye-Waller $B(T)$ factor has also been measured at ambient temperature, which suffices to determine the zero-point energy. The deviations from the standard Debye theory (regarding heat capacity, internal energy and entropy) in the intermediate temperature range are particularly pronounced in the case of rutile. We also calculate the molar internal energy and entropy of rutile over a wide temperature range as well as the temperature evolution of the $B(T)$ factor.

This method to infer the partition function and other thermodynamic functions from heat capacity data is widely applicable as it does not depend on microscopic structural details, nor does it require extensive numerical calculations. Apart from TiO_2 polymorphs [7,8], other possible applications include the heat capacity of magnetocaloric materials [9], chalcogenides [10,11], intermetallic compounds [12,13],

E-mail address: tom@geminga.org.

https://doi.org/10.1016/j.physb.2020.412243
Received 2 February 2020; Received in revised form 27 April 2020; Accepted 29 April 2020
Available online 14 May 2020

Heusler alloys [14], ceramics [15], and heavy-fermion systems [16,17]. Other attempts to find phenomenological caloric equations of state (EoSs) that can accurately reproduce experimental data, for instance, by adding Einstein oscillators to the Debye theory at optical frequencies or by assuming anharmonic perturbations of the oscillator potential, are discussed in Ref. [18–20] and references therein.

This paper is organized as follows. In Section 2, we introduce the varying Debye temperature $\theta(T)$ and spectral cutoff $\Lambda(T)$ in the partition function of the Debye theory in a way consistent with the mentioned equilibrium condition $\partial S/\partial U = 1/T$ and derive explicit analytic expressions for the internal energy, isochoric specific heat and entropy as functionals of the temperature-dependent spectral cutoff and Debye temperature.

In Section 3, we explain how to extract the temperature variation of the spectral cutoff $\Lambda(T)$ and Debye temperature $\theta(T)$ from heat capacity measurements. Both the internal energy $U(T)$ and entropy $S(T)$ are obtained from an analytic least-squares fit of the isochoric heat capacity and subsequent temperature integrations. These two variables $U(T)$, $S(T)$ depend on the Debye temperature and the spectral cutoff and thus define a system of two nonlinear equations for $\theta(T)$ and $\Lambda(T)$. This system always admits a unique solution and we show how to calculate it in practice. Asymptotic expressions for the low- and high-temperature limits of the Debye temperature and the spectral cutoff are obtained as well in this section, and we also compare with the Debye theory (which assumes a constant spectral cutoff and Debye temperature), especially with regard to the zero-point energy of the phonons.

In Section 4, a specific example is studied, the heat capacity, internal energy and entropy of rutile TiO_2. For this compound, several heat capacity measurements are available in the low- and high-temperature regimes as well as in the crossover region. A least-squares fit to the lattice heat capacity data of rutile is performed, using a multiply broken power-law density as fit function. By making use of the analytic expression for the isochoric heat capacity $C_V(T)$ obtained from the fit, we calculate the temperature variation of the entropy and the thermal component $U_{\rm therm}(T)$ of the internal energy, from the low-temperature regime up to the melting point.

In Section 5.1, we discuss the Debye-Waller B-factor, which has been measured for rutile by X-ray diffraction at ambient temperature, and explain how to extract the zero-point internal energy U_0 from the measured B-factor. As mentioned above, once the zero-point energy has been determined, one can use the internal energy $U(T) = U_{\rm therm}(T) + U_0$ and entropy $S(T)$ to calculate the temperature variation of the Debye temperature, the varying spectral cutoff and effective phonon speed defining the partition function, as well as the temperature dependence of the Debye-Waller factor $B(T)$. This is done for rutile TiO_2 in Section 5.2. In Section 6, we present our conclusions. A derivation of the effective phonon partition function, internal energy, entropy and Debye-Waller factor is sketched in Appendix A, to make this paper self-contained.

2. Thermodynamic variables and equilibrium condition for phonons

2.1. Temperature-dependent spectral cutoff

We start with the partition function Z of a Bose system of vibrational modes, cf. Appendix A,

$$\frac{\log Z}{V} = -\frac{4\pi\sigma}{(2\pi)^3}\int_0^{\Lambda(T,n)}\left(\log\left(1-\mathrm{e}^{-c_{\rm eff}(T,n)k/T}\right)+\frac{1}{2}\frac{c_{\rm eff}(T,n)k}{T}\right)k^2\mathrm{d}k, \tag{2.1}$$

where $c_{\rm eff}(T,n)$ is the effective phonon speed depending on temperature and atomic density n. The spectral cutoff $\Lambda(T,n)$ is likewise temperature and density dependent, and k labels the phonon wavenumber. The second term of the integrand is due to the zero-point energy of the phonons, arising in the bosonic quantization. Owing to the spectral cutoff, this term gives a finite contribution to the partition function (and internal energy). In (2.1), the same effective phonon speed $c_{\rm eff}(T,n)$ is used for transversal and longitudinal modes, defining the linear but temperature dependent dispersion relation $\omega = c_{\rm eff}(T,n)k$. The factor $\sigma = 3$ in (2.1) stems from the summation over the polarization states, cf. (A.12). For Z to be the partition function of an equilibrium system, $\Lambda(T,n)$ and $c_{\rm eff}(T,n)$ have to be interrelated because of their temperature dependence, as will be shown in Section 2.2. In the following, we will use the shortcut $\xi = \log Z/V$ and also refer to $\log Z$ and ξ as partition function. Eq. (2.1) can be derived by box quantization, sketched in Appendix A, and is identical to the partition function of the Debye theory where $\Lambda(T,n)$ and $c_{\rm eff}(T,n)$ are assumed to be constant.

We introduce a new integration variable in (2.1), $x = c_{\rm eff}(T,n)k/T$, and define the Debye temperature $\theta(T,n) = c_{\rm eff}(T,n)\Lambda(T,n)$ depending on the system temperature, to find $\log Z = V\xi$, where

$$\xi = -\frac{4\pi\sigma}{(2\pi)^3}\Lambda^3(T,n)\left[\frac{T^3}{\theta^3(T,n)}\int_0^{\theta(T,n)/T}\log(1-\mathrm{e}^{-x})x^2\mathrm{d}x+\frac{1}{8}\frac{\theta(T,n)}{T}\right]. \tag{2.2}$$

Integration by parts gives

$$\xi = \frac{4\pi\sigma}{(2\pi)^3}\frac{\Lambda^3}{3}\left[\frac{T^3}{\theta^3}\int_0^{\theta/T}\frac{x^3\mathrm{d}x}{\mathrm{e}^x-1}-\log\left(1-\mathrm{e}^{-\theta/T}\right)-\frac{3}{8}\frac{\theta}{T}\right]. \tag{2.3}$$

We will extensively use the Debye function

$$D(d) = \frac{1}{d^3}\int_0^d\frac{x^3\mathrm{d}x}{\mathrm{e}^x-1},\quad D'(d) = -\frac{3}{d}D(d)+\frac{1}{\mathrm{e}^d-1}, \tag{2.4}$$

and the shortcut $d = \theta(T,n)/T$. In this way, $\xi = \log Z/V$ can be written as

$$\xi = \frac{4\pi\sigma}{(2\pi)^3}\frac{1}{3}\Lambda^3\left[D(d)-\log\left(1-\mathrm{e}^{-d}\right)-\frac{3}{8}d\right], \tag{2.5}$$

and the temperature derivative thereof is

$$\begin{aligned}\xi_{,T} = \frac{4\pi\sigma}{(2\pi)^3}\Lambda^3\Big\{&(\log\Lambda)_{,T}\left[D(d)-\log\left(1-\mathrm{e}^{-d}\right)-\frac{3}{8}d\right]\\&+\left(\frac{1}{T}-(\log\theta)_{,T}\right)\left(D(d)+\frac{1}{8}d\right)\Big\}.\end{aligned} \tag{2.6}$$

2.2. Internal energy, isochoric heat capacity and entropy

The internal energy density reads, cf. (A.10),

$$u = \frac{U}{V} = \frac{4\pi\sigma}{(2\pi)^3}c_{\rm eff}(T,n)\int_0^{\Lambda(T,n)}\left(\frac{1}{\mathrm{e}^{c_{\rm eff}(T,n)k/T}-1}+\frac{1}{2}\right)k^3\mathrm{d}k. \tag{2.7}$$

Using the notation introduced in Section 2.1, we can write this as, cf. (2.4),

$$u(T,n) = \frac{4\pi\sigma}{(2\pi)^3}\Lambda^3 T\left(D(d)+\frac{d}{8}\right), \tag{2.8}$$

with $d = \theta(T,n)/T$. The condition $\xi_{,T} = u/T^2$, cf. (2.6), implies that the internal-energy derivative of entropy is the reciprocal temperature, and the reverse holds true as well. That is, $S_{,U}(U,V) = 1/T$ with $S = \log Z + U/T$ is equivalent to $\xi_{,T} = u/T^2$, as can be checked by implicit differentiation. To see this, we invert the internal energy density $u = u(T,n)$ for T to obtain $T = T(u,n)$. Differentiation of the identity $u = u(T(u,n), n)$ with respect to u gives $T_{,u}(u,n) = 1/u_{,T}(T,n)$. The entropy density $s = S/V$ is related to the partition function $\xi = \log Z/V$ and the internal energy density $u = U/V$ by $s(T,n) = \xi(T,n) + u(T,n)/T$, cf. after (A.11). The (u,n) parametrization thereof reads $s(u,n) = \xi(T(u,n),n) + u/T(u,n)$. (There is no chemical potential in the phonon partition function (2.1).) Differentiating this with respect to u gives $s_{,u} = (\xi_{,T} - u/T^2)/u_{,T} + 1/T$.

Since $S_{,U}(U,V) = s_{,u}(u,n)$ (with atomic density $n \propto 1/V$), the equilibrium condition $S_{,U} = 1/T$ is equivalent to $\xi_{,T} = u/T^2$.

More explicitly, condition $\xi_{,T} = u/T^2$ reads, with $\xi_{,T}$ in (2.6) substituted,

$$(\log\Lambda)_{,T} = (\log\theta)_{,T}\frac{D(d)+d/8}{D(d)-\log(1-\mathrm{e}^{-d})-3d/8}. \tag{2.9}$$

Eq. (2.9) is a necessary condition for partition function (2.1) to define an equilibrium system. If both the Debye temperature $\theta(T,n)$ and the cutoff $\Lambda(T,n)$ are independent of the system temperature, the equilibrium condition (2.9) is evidently satisfied, whereas a constant cutoff Λ and a varying $\theta(T,n)$ violate (2.9). The integrated version of (2.9) is

$$\Lambda(T,n) = \Lambda(T_0,n)\exp\left(\int_{T_0}^{T}\frac{\theta_{,T}}{\theta}\frac{D(d)+d/8}{D(d)-\log(1-\mathrm{e}^{-d})-3d/8}\mathrm{d}T\right). \tag{2.10}$$

Thus, the temperature variation of the spectral cutoff $\Lambda(T,n)$ is determined by the Debye temperature $\theta(T,n)$, apart from an integration constant $\Lambda(T_0,n)$.

The isochoric heat capacity $C_V = Vu_{,T}$ (or $c_V = u_{,T}$ with $c_V = C_V/V$) is the temperature derivative of energy density (2.8),

$$\begin{aligned}u_{,T} = {}&\frac{4\pi\sigma}{(2\pi)^3}\Lambda^3\left[4D(d)-\frac{d}{\mathrm{e}^d-1}+3T(\log\Lambda)_{,T}\left(D(d)+\frac{d}{8}\right)\right.\\&\left.-T(\log\theta)_{,T}\left(3D(d)-\frac{d}{8}-\frac{d}{\mathrm{e}^d-1}\right)\right],\end{aligned} \tag{2.11}$$

with $(\log\Lambda)_{,T}$ and Λ as stated in (2.9) and (2.10). The two logarithmic temperature derivatives in (2.11) vanish if $\theta(T,n)$ is temperature independent. In the above equations, the $d/8$ terms are manifestations of the zero-point energy in (2.1). As for the first two terms in (2.11), we may write, using integration by parts,

$$4D(d)-\frac{d}{\mathrm{e}^d-1} = \frac{1}{d^3}\int_0^d\frac{x^4\mathrm{e}^x\mathrm{d}x}{(\mathrm{e}^x-1)^2}. \tag{2.12}$$

As mentioned after (2.8), the entropy density $s = S/V$ is related to the partition function $\xi = \log Z/V$ and the internal energy density u by $s = \xi + u/T$. Thus, cf. (2.5) and (2.8),

$$s = \frac{4\pi\sigma}{(2\pi)^3}\Lambda^3\left[\frac{4}{3}D(d)-\frac{1}{3}\log\left(1-\mathrm{e}^{-d}\right)\right]. \tag{2.13}$$

The zero-point $d/8$ terms in the partition function and internal energy cancel each other here.

The isochoric heat capacity is related to the internal energy and entropy by $u = \int_0^T c_V\mathrm{d}T + u_0$ and $s = \int_0^T(c_V/T)\mathrm{d}T + s_0$, where u_0 and s_0 are integration constants; the equilibrium condition $\xi_{,T} = u/T^2$ is met by calculating u and s in this way, since $s = \xi + u/T$.

The effective phonon density (phonons per unit volume) can be read off from the integral representation (2.7) of the energy density, by dividing the integrand by the phonon energy $\omega = c_{\mathrm{eff}}(T,n)k$, see also (A.11) for a more formal derivation,

$$\frac{\langle N_{\mathrm{ph}}\rangle}{V} = \frac{4\pi\sigma}{(2\pi)^3}\int_0^{\Lambda(T,n)}\left(\frac{1}{\mathrm{e}^{c_{\mathrm{eff}}(T,n)k/T}-1}+\frac{1}{2}\right)k^2\mathrm{d}k. \tag{2.14}$$

The effective oscillator density at a given temperature is thus $N_{\mathrm{oscil}}/V = (4\pi\sigma/(2\pi)^3)\Lambda^3(T,n)/3$, obtained by replacing the expression in parentheses in the integrand of (2.14) by one; see also after (A.11) for the discrete version of N_{oscil} in box quantization and the thermodynamic limit.

2.3. Restoring units and conversion to molar quantities

In the previous sections, $\hbar = k_{\mathrm{B}} = 1$. We will use J/K units for $C_V = Vu_{,T}$, cf. (2.11), and J/(K cm^3) for the temperature derivative of the internal energy density $u_{,T}$. For the spectral cutoff $\Lambda(T,n)$ in (2.1) and (2.7), 1/cm units will be used; n denotes the atomic density and $\Lambda(T,n)$ can be written as $\Lambda(T,n) = n^{1/3}h(T,n)$, with dimensionless cutoff factor $h(T,n)$. The effective oscillator density is thus $N_{\mathrm{oscil}}/V = (4\pi\sigma/(2\pi)^3)nh^3(T,n)/3$, cf. after (2.14). To restore the units of u in (2.8), $u_{,T}$ in (2.11) and s in (2.13), we have to add a factor k_{B} on the right-hand side of these equations.

The Debye temperature is $\theta[\mathrm{K}] = \hbar c_{\mathrm{eff}}(T,n)\Lambda(T,n)/k_{\mathrm{B}}$, with the effective phonon speed $c_{\mathrm{eff}}[\mathrm{cm/s}]$. The parameter $d = \theta/T = \hbar c_{\mathrm{eff}}\Lambda/(k_{\mathrm{B}}T)$ and the Debye function $D(d)$ are dimensionless. We also note $d = \hbar n^{1/3}c_{\mathrm{eff}}(T,n)h(T,n)/(k_{\mathrm{B}}T)$ and inversely,

$$c_{\mathrm{eff}}(T,n) = \frac{k_{\mathrm{B}}\theta(T,n)}{\hbar n^{1/3}h(T,n)}. \tag{2.15}$$

When comparing with experimental data, it will be necessary to convert densities to molar quantities. Assuming the number of molecules constituting the sample to be the Avogadro number N_{A}mol, we can write the atomic density as $n = n_{a/m}N_{\mathrm{A}}\mathrm{mol}/V$, where $n_{a/m}$ is the number of atoms per molecule or formula unit. The conversion of the above densities to molar quantities is done by multiplying the respective density with V/mol and substituting $n = n_{a/m}N_{\mathrm{A}}\mathrm{mol}/V$ for the atomic density.

To summarize, the caloric EoS (molar internal energy in units of J/mol) reads, cf. (2.8),

$$U = \frac{4\pi\sigma}{(2\pi)^3}n_{a/m}Rh^3T\left(D(d)+\frac{d}{8}\right), \tag{2.16}$$

and the molar isochoric heat capacity (in units of J/(K mol)), cf. (2.11), is

$$\begin{aligned}C_V = {}&\frac{4\pi\sigma}{(2\pi)^3}n_{a/m}Rh^3\left[4D(d)-\frac{d}{\mathrm{e}^d-1}+3T(\log h)_{,T}\left(D(d)+\frac{d}{8}\right)\right.\\&\left.-T(\log\theta)_{,T}\left(3D(d)-\frac{d}{8}-\frac{d}{\mathrm{e}^d-1}\right)\right],\end{aligned} \tag{2.17}$$

and the molar entropy (in units of J/(K mol)), cf. (2.13), reads

$$S = \frac{4\pi\sigma}{(2\pi)^3}n_{a/m}Rh^3\left[\frac{4}{3}D(d)-\frac{1}{3}\log\left(1-\mathrm{e}^{-d}\right)\right]. \tag{2.18}$$

Here, we use the gas constant $R = N_{\mathrm{A}}k_{\mathrm{B}} = 8.314$ J/(K mol), $\sigma = 3$, and the dimensionless cutoff factor

$$h(T,n) = h(T=\infty)\exp\left(-\int_T^\infty\frac{\theta_{,T}}{\theta}\frac{D(d)+d/8}{D(d)-\log(1-\mathrm{e}^{-d})-3d/8}\mathrm{d}T\right), \tag{2.19}$$

obtained from (2.10), where we have put $T_0 = \infty$ (which can be freely chosen) and interchanged the integration boundaries. The integration constant $h(T=\infty) = (6\pi^2)^{1/3}$ will be determined in Section 3.2, see after (3.12).

The dimensionless cutoff $h(T,n)$ is related to the effective phonon speed $c_{\mathrm{eff}}(T,n)$ as stated in (2.15), and the variables in (2.16)–(2.18) are related by, cf. after (2.13),

$$U = \int_0^T C_V\mathrm{d}T + U_0, \quad S = \int_0^T\frac{C_V}{T}\mathrm{d}T + S_0, \tag{2.20}$$

where U_0 and S_0 are integration constants, cf. after (4.2). In the following, we will put $S_0 = 0$, so that the entropy vanishes at zero temperature, see also after (5.6).

3. Extracting the temperature variation of the spectral cutoff and Debye temperature from heat capacity data

3.1. Reconstruction of $\theta(T)$ and $\Lambda(T)$

Once the isochoric heat capacity $C_V(T)$ has been determined from a least-squares fit, we can substitute $U(T)$ and $S(T)$ (obtained by integrating the heat capacity, cf. (2.20)) into Eqs. (2.16) and (2.18) and solve for $d(T)=\theta(T)/T$ and the cutoff parameter $h(T)$. More explicitly, $d(T)$ is obtained by inverting

$$\frac{3}{4}\frac{TS(T)}{U(T)}=\Delta(d),\qquad \Delta(d):=1-\frac{2\log(1-\mathrm{e}^{-d})+d}{8D(d)+d}, \tag{3.1}$$

and subsequently $h(T)$ via the internal energy (2.16). (From now on, the atomic density variable n in $\theta(T,n)$, $h(T,n)$, etc., will be suppressed.) The linear d term in the numerator and denominator of $\Delta(d)$ is due to the zero-point energy. In this way, we find the Debye temperature $\theta=Td(T)$, the effective phonon speed $c_{\mathrm{eff}}=d(T)k_{\mathrm{B}}T/(\hbar n^{1/3}h(T))$, cf. (2.15), and the spectral cutoff $\Lambda(T)=n^{1/3}h(T)$, see the beginning of Section 2.3.

The asymptotic limits of $\Delta(d)$ in (3.1) and its inverse Δ^{-1} can readily be calculated. For $d>>1$, the asymptotic limit of the Debye function is [21]

$$D(d)=\frac{\pi^4}{15}\frac{1}{d^3}+\mathrm{O}\big(\mathrm{e}^{-d}\big), \tag{3.2}$$

and thus, cf. (3.1),

$$\Delta(d)=\frac{8\pi^4}{15}\frac{1}{d^4}\left(1+\frac{8\pi^4}{15}\frac{1}{d^4}\right)^{-1}+\mathrm{O}\big(\mathrm{e}^{-d}/d\big). \tag{3.3}$$

The inversion of (3.3) reads

$$d=\Delta^{-1}(r)\sim\left(\frac{8\pi^4}{15}\frac{1-r}{r}\right)^{1/4},\qquad r(T):=\frac{3}{4}\frac{TS(T)}{U(T)}<<1, \tag{3.4}$$

up to exponentially small terms, so that $d>>1$ in this limit.

In the opposite regime, $d<<1$, the expansions of $D(d)$ and $\Delta(d)$ are [21]

$$D(d)=\frac{1}{3}-\frac{d}{8}+\frac{d^2}{60}-\mathrm{O}\big(d^4\big), \tag{3.5}$$

$$\Delta(d)=-\frac{3}{4}\log d+1+d^2\left(\frac{3}{80}\log d-\frac{1}{32}\right)+\mathrm{O}\big(d^4\log d\big), \tag{3.6}$$

and the inversion of $\Delta(d)$ in (3.6) reads

$$d=\Delta^{-1}(r)\sim\mathrm{e}^{-4(r-1)/3}\left[1-\mathrm{e}^{-8(r-1)/3}\left(\frac{1}{15}(r-1)+\frac{1}{24}\right)+\cdots\right], \tag{3.7}$$

where $d<<1$ and $r(T)=3TS/(4U)>>1$.

The function $\Delta(d)$ defined in (3.1) is monotonously decreasing, from infinity at $d=0$ to zero at $d=\infty$, so that Eq. (3.1) admits a unique solution by inversion of $\Delta(d)$ (provided that the left-hand side of (3.1) is positive). For this reason, the linear d terms in the numerator and denominator of $\Delta(d)$ (generated by the zero-point term in the partition function (2.1)) are essential. If they are dropped, $\Delta(d\to\infty)$ would converge to one rather than zero, and $\Delta(d)$ would always exceed one, whereas the left-hand side of (3.1) can drop below one. In contrast, since $\Delta(d)$ varies between infinity and zero and is strictly monotone, Eq. (3.1) has always a unique solution,

$$d(T)=\frac{\theta(T)}{T}=\Delta^{-1}\left(\frac{3}{4}\frac{TS(T)}{U(T)}\right), \tag{3.8}$$

with $S(T)$ and $U(T)$ in (2.20), and Δ^{-1} denotes the inverse of $\Delta(d)$ in (3.1). In this way, we find the Debye temperature $\theta(T)=Td(T)$ and also the spectral cutoff $h(T)$ by substituting $d(T)$ and $U(T)$ into (2.16),

$$h(T)=\left(\frac{(2\pi)^3}{4\pi\sigma}\frac{1}{n_{a/m}RT}\frac{U(T)}{D(d(T))+d(T)/8}\right)^{1/3}. \tag{3.9}$$

Both $d(T,U_0)$ in (3.8) and $h(T,U_0)$ in (3.9) depend on the zero-point energy U_0, since $U=\int_0^T C_V\mathrm{d}T+U_0$ and $S=\int_0^T C_V/T\mathrm{d}T$, where $C_V(T)$ is a least-squares fit to the measured lattice heat capacity, cf. (2.20).

3.2. High-temperature asymptotics of Debye temperature, spectral cutoff and effective phonon speed

In Sections 3.2 and 3.3, we derive the high- and low-temperature limits of the Debye temperature $\theta(T)$, cf. (3.8), the spectral cutoff $h(T)$, cf. (3.9), and the effective phonon speed $c_{\mathrm{eff}}(T)$, cf. (2.15). Since the lattice heat capacity approaches a constant in the classical high-temperature regime, $C_V\sim c_{V\infty}[\mathrm{J/(K\ mol)}]+\mathrm{O}(1/T^{\varepsilon})$, $\varepsilon>0$, we find $U(T)\sim c_{V\infty}T$ and, cf. (2.20),

$$\begin{aligned}&S(T)\sim c_{V\infty}\log T[\mathrm{K}]+s_{V\infty},\\ &s_{V\infty}:=\lim_{T\to\infty}\left(\int_0^{T[\mathrm{K}]}\frac{C_V(T)}{T}\mathrm{d}T-c_{V\infty}\log T[\mathrm{K}]\right),\end{aligned} \tag{3.10}$$

with constant $s_{V\infty}[\mathrm{J/(K\ mol)}]$, so that, cf. (3.1) and (3.6),

$$\Delta(d)\sim-\frac{3}{4}\log d+1\sim\frac{3}{4}\left(\log T+\frac{s_{V\infty}}{c_{V\infty}}\right), \tag{3.11}$$

with $d=\theta(T)/T<<1$. Thus $\theta(T)$ and $h(T)$ (the latter calculated via (3.9)) are constant in the high-temperature limit, as is the effective phonon speed (2.15),

$$\theta_{T\to\infty}\sim\exp\left(\frac{4}{3}-\frac{s_{V\infty}}{c_{V\infty}}\right),\ h_{T\to\infty}\sim\left(\frac{3(2\pi)^3}{4\pi\sigma}\frac{c_{V\infty}}{n_{a/m}R}\right)^{1/3},\ c_{\mathrm{eff},T\to\infty}=\frac{k_{\mathrm{B}}}{\hbar n^{1/3}}\frac{\theta_{T\to\infty}}{h_{T\to\infty}}. \tag{3.12}$$

The classical Dulong-Petit limit of the heat capacity is $c_{V\infty}=\sigma n_{a/m}R$, where $\sigma=3$ labels the vibrational degrees of freedom of each atom, and $n_{a/m}$ denotes the number of atoms in each molecule or formula unit, so that $h_{T\to\infty}\sim(6\pi^2)^{1/3}$, cf. (3.12). (The limits (3.12) do not depend on the zero-point energy U_0, cf. Section 3.3.) Accordingly, the effective oscillator density $N_{\mathrm{oscil}}/V=(4\pi\sigma/(2\pi)^3)nh^3(T)/3$ (cf. after (2.14) and the beginning of Section 2.3) converges to σn in the high-temperature limit, where n is the atomic density.

Finally, the high-temperature limits $d=\theta(T)/T<<1$ of the molar internal energy and entropy read, cf. (2.16), (2.18) and (3.5),

$$U=\frac{4\pi\sigma}{(2\pi)^3}n_{a/m}Rh^3T\left(\frac{1}{3}+\frac{d^2}{60}-\mathrm{O}\big(d^4\big)\right), \tag{3.13}$$

$$S=\frac{4\pi\sigma}{(2\pi)^3}n_{a/m}Rh^3\left(-\frac{1}{3}\log d+\frac{4}{9}+\frac{d^2}{120}+\mathrm{O}\big(d^4\big)\right). \tag{3.14}$$

3.3. Low-temperature limit of Debye temperature and spectral cutoff

In the low-temperature regime $d=\theta(T)/T>>1$, the Debye function (2.4) admits the asymptotic limit (3.2), so that, cf. (2.16),

$$U=\frac{4\pi\sigma}{(2\pi)^3}n_{a/m}Rh^3T\frac{d}{8}\left(1+\frac{8\pi^4}{15}\frac{1}{d^4}+\mathrm{O}\big(\mathrm{e}^{-d}/d\big)\right). \tag{3.15}$$

The leading order here is entirely due to the zero-point energy (the $d/8$ term in (2.16)). The asymptotic limit of the entropy (2.18) reads

$$S=\frac{4\pi\sigma}{(2\pi)^3}n_{a/m}Rh^3\left(\frac{4}{3}\frac{\pi^4}{15}\frac{1}{d^3}+\mathrm{O}\big(\mathrm{e}^{-d}\big)\right). \tag{3.16}$$

A consistency check is obtained by way of (3.1) and (3.3).

At low temperature, the heat capacity is assumed to be a power law, $C_V \sim c_{V0}T^\alpha$, $\alpha > 0$, with amplitude c_{V0}[J/(K$^{1+\alpha}$ mol)] and T[K]. Thus, according to (2.20), $S \sim c_{V0}T^\alpha/\alpha$ and $U \sim c_{V0}T^{\alpha+1}/(\alpha+1) + U_0$. We have put $S_0 = 0$, for the entropy to vanish at zero temperature, and c_{V0} and U_0 are positive constants. In leading order, cf. (3.3),

$$\Delta(d) \sim \frac{8\pi^4}{15}\frac{1}{d^4} \sim \frac{3}{4}\frac{c_{0V}T^{\alpha+1}}{\alpha U_0}, \tag{3.17}$$

for $d = \theta(T)/T >> 1$. The Debye temperature (via (3.17)) and the cutoff factor $h(T)$ (via (3.15)) thus scale as

$$\theta_{T\to 0} \sim \left(\frac{32\pi^4}{45}\frac{\alpha U_0}{c_{0V}}\right)^{1/4} T^{(3-\alpha)/4}, \quad h_{T\to 0} \sim \left(\frac{8(2\pi)^3}{4\pi\sigma}\frac{U_0}{n_{a/m}R}\frac{1}{\theta_{T\to 0}}\right)^{1/3}, \tag{3.18}$$

in the low-temperature regime and are temperature independent for $\alpha = 3$, provided that the integration constant U_0 of the internal energy in (2.20) is positive. The low-temperature limit of the effective phonon speed reads, cf. (2.15),

$$c_{\mathrm{eff},T\to 0} = \frac{k_\mathrm{B}}{\hbar n^{1/3}}\frac{\theta_{T\to 0}}{h_{T\to 0}} = \frac{k_\mathrm{B}}{\hbar n^{1/3}}\left(\frac{4\pi\sigma}{(2\pi)^3}\frac{4\pi^4}{45}n_{a/m}R\frac{\alpha}{c_{0V}}\right)^{1/3} T^{(3-\alpha)/3}, \tag{3.19}$$

which is independent of the integration constant U_0 and constant for $\alpha = 3$ (power-law exponent of the specific heat, cf. after (3.16)).

3.4. Comparison with the Debye approximation

The Debye formula for the molar heat capacity is recovered by assuming a constant Debye temperature θ and a constant spectral cutoff h, see (2.17) (and also (2.12)),

$$C_V = \frac{4\pi\sigma}{(2\pi)^3}n_{a/m}Rh^3\left[4D(\theta/T) - \frac{\theta/T}{e^{\theta/T}-1}\right], \tag{3.20}$$

$$\theta = \left(\frac{4\pi^4\sigma}{5}\frac{n_{a/m}R}{c_{0V}}\right)^{1/3}, \quad h = (6\pi^2)^{1/3}. \tag{3.21}$$

Here, $C_V \sim c_{V0}T^3$, cf. Section 3.3, and $\sigma = 3$. The units are c_{V0}[J/(K^4 mol)], T[K] and C_V[J/(K mol)]. The zero-point contributions to the heat capacity (which are the $d/8$ terms in (2.17)) drop out if the temperature derivatives of θ and h vanish, but the zero-point energy of the phonons does show in the internal energy (2.16), which admits a finite zero-temperature limit U_0, cf. (3.15),

$$U_0 = \frac{4\pi\sigma}{(2\pi)^3}n_{a/m}Rh^3\frac{\theta}{8} = \left(\frac{32\pi^4}{15}\right)^{1/3}\left(\frac{3\sigma}{8}\right)^{4/3}\frac{(n_{a/m}R)^{4/3}}{c_{0V}^{1/3}}. \tag{3.22}$$

A consistency check is obtained by integrating $C_V(T)$ in (3.20) and comparing with $U(T)$ in (2.16) and (2.20),

$$\int_0^T C_V\mathrm{d}T = \frac{4\pi\sigma}{(2\pi)^3}n_{a/m}Rh^3TD(d), \tag{3.23}$$

where we used (2.12) and integration by parts and $d = \theta/T$. Analogously, $S(T) = \int_0^T (C_V/T)\mathrm{d}T$, cf. (2.20), with $C_V(T)$ in (3.20), $S(T)$ in (2.18) and constant θ and h. Using the high-temperature limit of $S(T)$ in (3.14) with (3.21) substituted, we find, by comparing with $S \sim c_{V\infty}\log T + s_{V\infty}$ in (3.10),

$$c_{V\infty} = \sigma n_{a/m}R, \qquad s_{V\infty} = \sigma n_{a/m}R\left(\frac{4}{3} - \log\theta\right), \tag{3.24}$$

consistent with $\theta_{T\to\infty}$ in (3.12). Finally, the effective phonon speed (2.15) reads, cf. (3.21),

$$c_\mathrm{eff} = \frac{k_\mathrm{B}}{\hbar n^{1/3}}\left(\frac{2\pi^2\sigma}{15}\frac{n_{a/m}R}{c_{0V}}\right)^{1/3}, \tag{3.25}$$

in accordance with the asymptotic limits of c_eff in (3.12) and (3.19); n denotes the atomic density.

The molar zero-point energy U_0 in (3.22) can be quite large (as compared with the thermal component of the internal energy); in the case of the rutile polymorph of TiO_2, $U_{0,\mathrm{Debye}} = 2.179\times 10^4$ J/mol, calculated with $\theta = 776.6$ K and $c_{0V} = 1.245\times 10^{-5}$ J/(K^4 mol). These estimates are based on the standard Debye heat capacity as defined in (3.20) and (3.21). The zero-point energy U_0 in the Debye theory is not a free integration constant, but already determined by the constant Debye temperature and spectral cutoff. This is in contrast to the internal energy adapted to a varying Debye temperature $\theta(T)$, which depends on U_0 as an integration constant, cf. (2.16), (2.20) and Section 3.1; the latter can be determined by measuring the Debye-Waller B-factor, cf. Section 5.

4. Heat capacity of titanium dioxide (rutile polymorph)

We perform a χ^2 fit to the available data sets [22–25] of the rutile TiO_2 heat capacity, depicted in the double-logarithmic plot in Fig. 1, by employing a multiply broken power law [26–28] as molar isochoric heat capacity,

$$C_V(T) = b_0T^{\beta_0}\left(1+(T/b_1)^{\beta_1/\eta_1}\right)^{\eta_1}\frac{1}{\left(1+(T/b_2)^{\beta_2/\eta_2}\right)^{\eta_2}}\frac{1}{\left(1+(T/b_3)^{\beta_3/\eta_3}\right)^{\eta_3}}, \tag{4.1}$$

with positive amplitudes b_0 and $b_1 < b_2 < b_3$. The exponents β_i and η_i are positive, and

$$b_3 = \left(9R\frac{b_1^{\beta_1}}{b_2^{\beta_2}b_0}\right)^{1/\beta_3}, \quad \beta_0 = 3, \quad \beta_3 = \beta_0+\beta_1-\beta_2, \tag{4.2}$$

so that the classical Dulong-Petit limit $C_V(T\to\infty) \sim 9R$ is recovered, with gas constant $R = 8.314$ J/(K mol). The low-temperature limit is $C_V(T\to 0) \sim b_0T^3$; the units used are C_V[J/(K mol)], b_0[J/(K^4 mol)] and b_i[K], cf. Section 2.3.

Broken power laws composed of multiple factors $\left(1+(T/b_i)^{\beta_i/|\eta_i|}\right)^{\eta_i}$ are quite efficient for data sets extending over several logarithmic decades in temperature. In (4.1), there are four successive power laws, $\propto T^3$, $T^{3+\beta_1}$, $T^{3+\beta_1-\beta_2}$, 1, in the intervals $T << b_1$, $b_1 << T << b_2$, $b_2 << T << b_3$ and $b_3 << T$, respectively, and the exponents η_i determine the curvature in the transitional regions around the break points b_i. The independent fitting parameters $b_{0,1,2}$, $\eta_{1,2,3}$ and $\beta_{1,2}$, obtained from the least-squares fit of $C_V(T)$ in (4.1) to the data sets, are recorded in Table 1. In contrast to the Debye approximation of the heat capacity, cf. (3.20) and (3.21), the heat capacity of rutile has an inflection point (in log-log representation) in the crossover region between the low- and high-temperature regimes, see Fig. 1; the tangent of C_V at the inflection point is depicted as green dotted line $\propto T^{5.159}$. $C_V(T)$ is plotted in Fig. 1 up to the melting point of 2116 K.

As for the Debye approximation, also depicted in Fig. 1, the amplitude c_{0V} in (3.21) is taken from the least-squares fit of $C_V(T)$ in (4.1), $c_{0V} = b_0$, cf. Table 1, to recover the cubic low-temperature slope. Accordingly, the Debye temperature (4.21) of rutile is $\theta = 776.6$, but the Debye approximation becomes inaccurate in the crossover region, where a pronounced phonon peak emerges in the second logarithmic decade in Fig. 1.

Based on the Debye theory, the constant effective phonon speed in rutile is $c_{\mathrm{eff,Debye}} = 5.703\times 10^5$cm/s, where we used (3.25) (with $\sigma = n_{a/m} = 3$) and the atomic density $n_\mathrm{rutile} = 9.569\times 10^{22}$ /cm^3. The

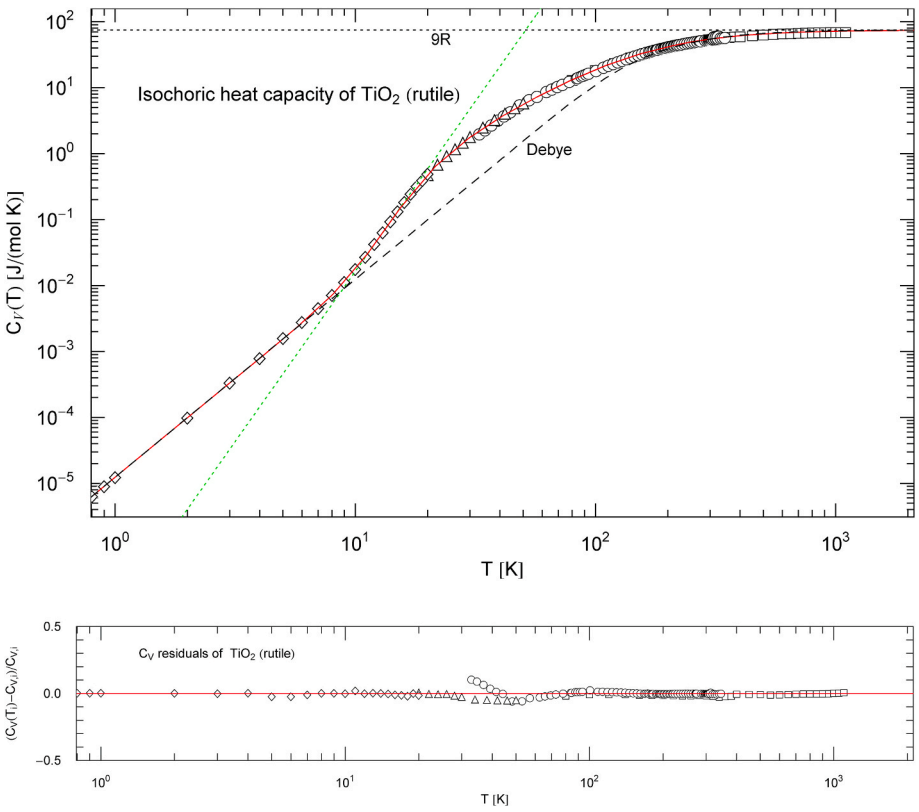

Fig. 1. Isochoric heat capacity of rutile. Data points from Ref. [22] (squares), Ref. [23] (circles), Ref. [24] (triangles) and Ref. [25] (diamonds). The least-squares χ^2 fit (solid red curve) is performed with the multiply broken power law $C_V(T)$ in (4.1), the fitting parameters are stated in Table 1. The classical $9R$ Dulong-Petit limit is indicated by the black dotted line. For comparison, the black dashed curve is the Debye approximation (3.20) with constant Debye temperature $\theta = 776.6$ K, which reproduces the low-temperature T^3 slope and the constant $9R$ high-temperature limit of $C_V(T)$ but is largely off the mark in the crossover region. The green dotted straight line depicts the tangent cT^κ at the inflection point ($T = 13.27$ K, $C_V = 0.07106$ J/(mol K)), with slope $\kappa = 5.159$ and amplitude $c = 1.143 \times 10^{-7}$ J/(mol K$^{1+\kappa}$), leading to an extended phonon peak stretching over the second logarithmic temperature decade. Residuals of the χ^2 fit are depicted in the lower panel. (For interpretation of the references to colour in this figure legend, the reader is referred to the Web version of this article.)

Table 1
Fitting parameters of the molar isochoric heat capacity $C_V(T)$ of rutile. The recorded amplitudes b_i and exponents β_i, η_i define the multiply broken power law (4.1) used for the χ^2 fit in Fig. 1. Some of the parameters in (4.1) are interrelated, in particular $\beta_0 = 3$ (defining the cubic low-temperature slope) and $\beta_3 = \beta_0 + \beta_1 - \beta_2$ as well as the amplitudes b_i, cf. (4.2). $\chi^2 = \sum_{i=1}^N (C_V(T_i) - C_{Vi})^2 / C_{Vi}^2$ denotes the minimum of the least-squares functional; the degrees of freedom (dof: number N of data points (T_i, C_{Vi}) minus number of independent fitting parameters) are also listed. SE $= \left(\sum_{i=1}^N (C_V(T_i) - C_{Vi})^2/N\right)^{1/2}$ is the standard error of the fit. The coefficient of determination, $R^2 = 1 - \sum_{i=1}^N (C_V(T_i) - C_{Vi})^2/(N\sigma^2)$, with sample variance $\sigma^2 = \sum_{i=1}^N (C_{Vi} - \overline{C}_V)^2/N$ and mean $\overline{C}_V = \sum_{i=1}^N C_{Vi}/N$, is recorded as well.

b_0[J/(K$^{1+\beta_0}$ mol)]	b_1[K]	b_2[K]	b_3[K]	β_1	β_2	η_1	η_2	η_3	χ^2	dof	SE	$1 - R^2$
1.2449×10^{-5}	10.966	15.148	155.02	7.6961	8.5594	1.6528	2.3513	1.1828	0.0545	152 − 8	0.256	1.11×10^{-4}

temperature-dependent effective phonon speed $c_{\rm eff}(T)$ consistent with the empirical heat capacity and the Debye-Waller factor measured at ambient temperature will be discussed in Section 5.

5. Debye-Waller *B*-factor and zero-point vibrations

5.1. Extracting the zero-point energy from B-factor measurements

The Debye-Waller intensity factor is e^{-2M}, with $M = B\sin^2\theta/\lambda^2$ and B-factor $B[\text{Å}^2] = 8\pi^2\langle u_Q^2\rangle$, where λ denotes the wavelength of the incident X-rays, 2θ is the scattering angle, and $\langle u_Q^2\rangle$ the atomic mean-squared displacement (parallel to the diffraction vector $\mathbf{Q}$) due to thermal and zero-point vibrations. $\langle u_Q^2\rangle$ is calculated as, cf., e.g., Ref. [29] and Appendix A,

$$\langle u_Q^2\rangle = \frac{A}{mN_{\rm oscil}}, \quad A := \frac{4\pi\sigma}{(2\pi)^3}\frac{V}{c_{\rm eff}(T)}\int_0^{\Lambda(T)}\left(\frac{1}{e^{c_{\rm eff}(T)k/T}-1}+\frac{1}{2}\right)k\,dk, \tag{5.1}$$

where $N_{\rm oscil}$ is the effective oscillator number, see after (2.14) and the beginning of Section 2.3, m is the averaged atomic mass (i.e. oscillator mass, see the end of Appendix A), $c_{\rm eff}(T)$ the effective phonon speed, $\Lambda(T)$ the spectral cutoff, and $\theta(T) = c_{\rm eff}(T)\Lambda(T)$ the varying Debye temperature, cf. Section 2.1. This is the same definition of the B-factor as in the standard Debye theory, apart from the temperature dependence of the Debye temperature $\theta(T)$ and spectral cutoff $\Lambda(T)$. The oscillator mass m does not enter in the thermodynamic variables discussed in Section 2.

The numerator in (5.1) can be written as

$$A = \frac{4\pi\sigma}{(2\pi)^3}\frac{\Lambda^3 T}{\theta^2}V\left(D_1(d)+\frac{d}{4}\right), \quad D_1(d) := \frac{1}{d}\int_0^d \frac{x\,dx}{e^x-1}, \tag{5.2}$$

with $d = \theta(T)/T$. Using $\Lambda(T)$ and $N_{\rm oscil}/V$ as defined in Section 2.3, and multiplying the right-hand side of Eq. (5.2) by $\hbar^2/k_{\rm B}$ to restore the units, we find the mean-squared vibrational displacement as

$$\langle u_Q^2\rangle = \frac{3}{m}\frac{\hbar^2 T}{k_{\rm B}\theta^2(T)}\left(D_1(d)+\frac{d}{4}\right), \tag{5.3}$$

where $d = \theta(T)/T$. Evidently, $\langle u_Q^2\rangle = A/(mN_{\rm oscil})$ only depends on the Debye temperature $\theta(T)$, since the cutoff factor $\Lambda^3(T)$ in (5.2) is cancelled by $N_{\rm oscil}$, cf. after (2.14). The asymptotic limits of the Debye function $D_1(d)$ in (5.2) and (5.3) are [21]

$$D_1(d) = \frac{\pi^2}{6}\frac{1}{d} + O(e^{-d}), \quad D_1(d) = 1 - \frac{d}{4} + \frac{d^2}{36} + O(d^4), \tag{5.4}$$

valid for $d >> 1$ and $d << 1$, respectively. Accordingly, the asymptotic limits of $\langle u_Q^2\rangle$ for large and small $d = \theta(T)/T$ read

$$\langle u_Q^2\rangle = \frac{3}{m}\frac{\hbar^2}{k_B\theta}\frac{1}{4}\left(1+\frac{2\pi^2}{3d^2}+\mathrm{O}\left(\mathrm{e}^{-d}/d\right)\right), \tag{5.5}$$

$$\langle u_Q^2\rangle = \frac{3}{m}\frac{\hbar^2 T}{k_B\theta^2}\left(1+\frac{d^2}{36}+\mathrm{O}(d^4)\right). \tag{5.6}$$

Since $\theta(T)$ approaches a constant at high temperature, cf. (3.12), we find $\langle u_Q^2\rangle \propto T$ in this limit (assuming a temperature-independent oscillator mass, cf. the end of Section 5.2). At low temperature, $\theta(T)$ is also temperature independent, cf. (3.18), as is $\langle u_Q^2\rangle$ in this limit, cf. (5.5). At low temperature, the Debye temperature depends on the zero-point energy, $\theta(T)\propto U_0^{1/4}$, cf. (2.20) and (3.18), so that $\langle u_Q^2\rangle \propto U_0^{-1/4}$ in the low-temperature regime. By the way, the cubic low-temperature scaling $C_V\propto T^\alpha$, $\alpha = 3$, cf. Section 3.3, is essential to obtain a finite low-temperature limit of $\langle u_Q^2\rangle$. For any other choice of the exponent α, the mean-squared vibrational amplitude would either diverge for $T\to 0$ or converge to zero (which is not possible either because of the uncertainty principle). A finite residual zero-point entropy S_0, cf. (2.20), would also result in a divergent $\langle u_Q^2\rangle$, since $\theta_{T\to 0}\propto T$ in this case.

The B-factor $8\pi^2\langle u_Q^2\rangle$ can be assembled as, cf. (5.3),

$$B(T)\left[\text{Å}^2\right] = 1.14903\times 10^4\frac{1}{m[\mathrm{u}]T[\mathrm{K}]}\frac{1}{d^2}\left(D_1(d)+\frac{d}{4}\right), \tag{5.7}$$

where m[u] is the averaged atomic mass in atomic mass units. We substitute $d(T,U_0) = \Delta^{-1}(3TS/(4U))$ (cf. (3.8)) into (5.7), with $U(T)[\mathrm{J/\ mol}] = \int_0^T C_V(T)\mathrm{d}T + U_0$ and $S(T)[\mathrm{J/(K\ mol)}] = \int_0^T C_V(T)/T\mathrm{d}T$ as defined in (2.20), where $C_V(T)$ is the analytic fit (4.1) to the empirical lattice heat capacity. By measuring the B-factor at a given temperature, one can thus determine the zero-point energy by solving (5.7) for U_0, which will be done in Section 5.2 for the rutile polymorph of TiO_2. For compounds, we use the mean B-factor of the constituents and, in the case of non-cubic symmetry, also isotropize by averaging the B-factors of the measured vibrational projections $\langle u_Q^2\rangle$.

5.2. B-factor, zero-point energy, internal energy and entropy of rutile

As for the mean B-factor of rutile TiO_2, we use (5.7) with average atomic mass of $m = 26.622$ u (based on 15.999 u for oxygen and 47.867 u for titanium) to find

$$B_{\mathrm{rutile}}(T)\left[\text{Å}^2\right] = 431.614\frac{1}{T[\mathrm{K}]}\frac{1}{d^2}\left(D_1(d)+\frac{d}{4}\right), \tag{5.8}$$

where $d(T,U_0) = \theta(T,U_0)/T$ is defined after (5.7), with the measured heat capacity of rutile represented by the analytic fit $C_V(T)$ in (4.1). A mean-squared displacement $\langle u_Q^2\rangle$ of 0.0065 Å^2 was measured for rutile in Ref. [30], implying a B-factor of 0.513 Å^2 at ambient temperature of 298.15 K. Solving (5.8) for U_0 gives a zero-point energy of $U_0 = 1.164\times 10^4$ J/mol, the unique solution of (5.8), which is by almost a factor of two smaller than $U_{0,\mathrm{Debye}}$ obtained with constant Debye temperature, see after (3.25).

The temperature dependence of the molar internal energy $U(T)$ and entropy $S(T)$ of rutile, cf. (2.20) and after (5.7) (with $S_0 = 0$, zero-point energy $U_0 = 1.164\times 10^4$ J/mol and $C_V(T)$ in (4.1) and Table 1), is shown in Fig. 2. The variation of the Debye temperature $\theta(T) = Td(T,U_0)$ is found as $\theta(T) = T\Delta^{-1}((3/4)TS(T)/U(T))$ (cf. (3.8) and after (5.7)) and depicted in Fig. 3. The spectral cutoff $h(T)$ in the partition function is calculated via (3.9) (with $U(T)$ and $d(T,U_0)$ substituted), see Fig. 4, and the effective phonon speed $c_{\mathrm{eff}}(T)$ via (2.15), see Fig. 5. The estimate of $c_{\mathrm{eff}}(T)$ is obtained with the atomic density $n_{\mathrm{rutile}} = 9.569\times 10^{22}$ /cm^3 (based on a mass density of 4.23 g/cm^3 and a molar mass of 79.87 g/mol), which gives the amplitude $k_B/(\hbar n_{\mathrm{rutile}}^{1/3}) = 2.862\times 10^3$cm/(s K) in (2.15). Finally, by specifying $U_0 = 1.164\times 10^4$ J/mol in $d(T,U_0)$, we find the temperature dependence of $B_{\mathrm{rutile}}(T)$ via (5.8), see Fig. 6, which is consistent with the measured $B_{\mathrm{rutile}} = 0.513$ Å^2 at 298.15 K. Fig. 6 also shows the temperature variation of the Debye-Waller factor of the Debye theory (based on (5.8) with constant $\theta = 776.6$ K, cf. after (3.25)), which substantially underestimates the measured B-factor at 298.15 K.

For most compounds and even elemental crystals, X-ray or neutron diffraction measurements of B-factors have only been done at ambient temperature, cf., e.g., Refs. [32,33] and references therein. For a few metals, such as Cu, Al, Pb, Ag, Au, Pt, a limited number of low- and high-temperature B-factors have been measured, cf., e.g., Refs. [34,35], but usually one has to content with the ambient B-factor, that is, with one single data point. This is the case for rutile, and this data point suffices to estimate the zero-point energy as pointed out above. The available data point is indicated in Fig. 6, and the zero-point energy is chosen so that the $B(T)$ curve (5.8) passes through this point.

If there are several low- and high-temperature data points $(T_i, B(T_i))$ available, one can perform a polynomial least-squares fit up to the melting point, insert the regressed $B(T)$ into Eq. (5.7) and replace the averaged atomic mass m[u] by an effective temperature-dependent oscillator mass $m(T)$[u] obtained by solving (5.7). The zero-point energy U_0 is determined by the boundary condition that this effective mass coincides with the atomic mass at zero temperature, and the varying Debye temperature and spectral cutoff are calculated as indicated above.

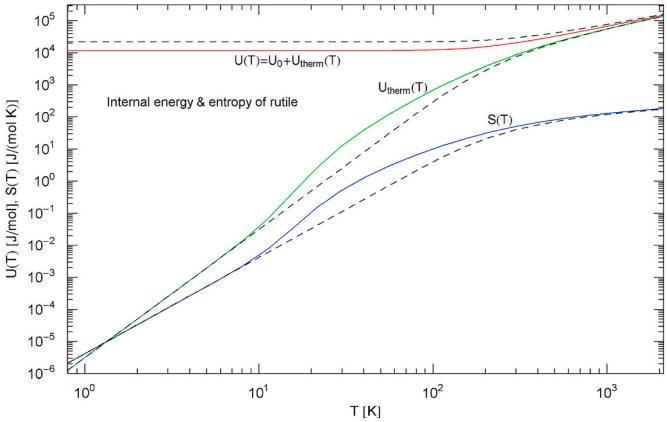

Fig. 2. Caloric EoS $U(T) = \int_0^T C_V\mathrm{d}T + U_0$ and molar entropy $S(T) = \int_0^T (C_V/T)\mathrm{d}T$ of rutile, cf. (2.20). The regressed heat capacity $C_V(T)$ in the integrands is stated in (4.1), with fitting parameters in Table 1, see Fig. 1. The caloric EoS (molar internal energy, including the zero-point energy $U_0 = 1.164\times 10^4$ J/mol extracted from the measured Debye-Waller B-factor, cf. Section 5.2) is depicted as red solid curve, its thermal component $U_{\mathrm{therm}}(T) = \int_0^T C_V\mathrm{d}T$ as green solid curve, and the molar entropy as blue solid curve. At high temperature, $U(T)\propto T$, and the entropy diverges logarithmically, cf. Section 3.2. The low-temperature slopes are $U_{\mathrm{therm}}(T)\propto T^4$ and $S(T)\propto T^3$, cf. Section 3.3. The black dashed curves show the Debye approximations of $U(T)$, $U_{\mathrm{therm}}(T)$ and $S(T)$, based on the Debye heat capacity (3.20) (with constant $\theta = 776.6$ K) and the Debye zero-point energy of rutile, $U_{0,\mathrm{Debye}} = 2.179\times 10^4$ J/ mol, cf. after (3.25). The phonon peak in the second temperature decade, cf. Fig. 1, is also clearly visible in $U_{\mathrm{therm}}(T)$ and $S(T)$. The zero-point energy $U_{0,\mathrm{Debye}}$ predicted by the Debye theory with constant $\theta = 776.6$ K is by almost a factor of two larger than the zero-point energy $U_0 = 1.164\times 10^4$ J/mol consistent with the measured B-factor of rutile, cf. Section 5.2. (For interpretation of the references to colour in this figure legend, the reader is referred to the Web version of this article.)

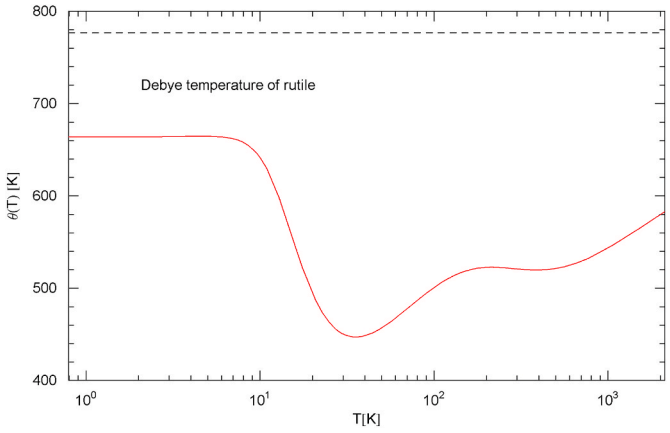

Fig. 3. Debye temperature of rutile. The temperature dependence of the Debye temperature $\theta(T)$ (red solid curve) is calculated from the temperature variation of the internal energy and entropy, via $\theta(T) = T\Delta^{-1}((3/4)TS/U)$, cf. (3.8), where $U(T) = \int_0^T C_V \mathrm{d}T + U_0$ and $S(T) = \int_0^T (C_V/T)\mathrm{d}T$, and Δ^{-1} denotes the inverse of $\Delta(d)$ in (3.1). The analytic fit $C_V(T)$ of the molar heat capacity of rutile is stated in (4.1) with parameters in Table 1, cf. Fig. 1. $\theta(T)$ approaches constant limit values at low and high temperature, cf. (3.12) and (3.18); the constant high-temperature limit is not attained within the solid phase. (In all figures, the temperature range is cut off at the melting point of rutile, at 2116 K.) The black dashed straight line indicates the constant Debye temperature $\theta = 776.6$ K used in the Debye approximations depicted in Figs. 1 and 2, cf. after (3.25). (For interpretation of the references to colour in this figure legend, the reader is referred to the Web version of this article.)

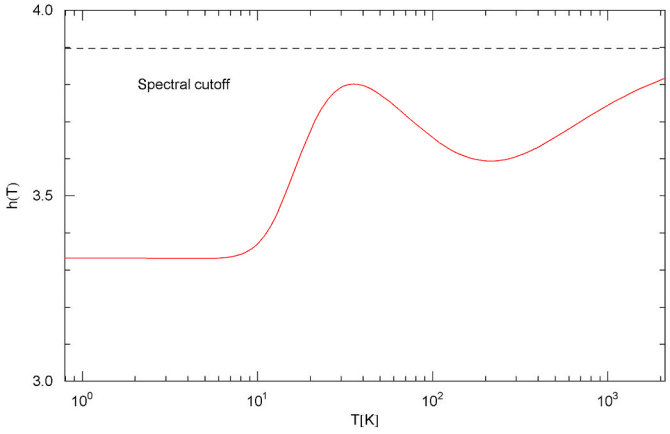

Fig. 4. Spectral cutoff in the partition function of rutile. The cutoff $\Lambda(T) = n^{1/3}h(T)$ of $\log Z$ in (2.1) depends on the atomic density of rutile, $n_{\mathrm{rutile}} = 9.569 \times 10^{22}$ /cm^3, and a dimensionless cutoff factor $h(T)$ (red solid curve), cf. Section 2.3. $h(T)$ is calculated from the internal energy $U(T)$ and the Debye temperature $\theta(T)$, cf. Figs. 2 and 3, by way of (3.9). Both the low- and high-temperature limits of $h(T)$ are constant, cf. (3.12) and (3.18). At high temperature, $h(T)$ converges to the constant cutoff factor of the Debye approximation, $h_{\mathrm{Debye}} = (6\pi^2)^{1/3}$, depicted here as black dashed straight line, cf. (3.12) and (3.21). (This convergence is not visible in the temperature range shown in this figure, as it happens above the melting point.) In the low-temperature regime, $h(T)$ depends on the zero-point energy U_0, cf. (3.18), inferred from a measurement of the Debye-Waller B-factor, cf. Section 5. (For interpretation of the references to colour in this figure legend, the reader is referred to the Web version of this article.)

6. Conclusion

The Debye theory of heat capacity reproduces the correct low- and high-temperature limits and is very practical, but in the intermediate temperature range it is not very accurate, see the double-logarithmic

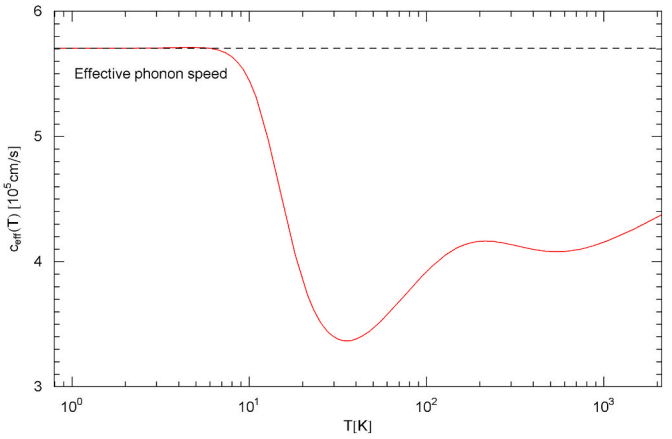

Fig. 5. Effective phonon speed of rutile. $c_{\mathrm{eff}}(T)$ is calculated from the Debye temperature in Fig. 3 and the spectral cutoff $h(T)$ in Fig. 4 by way of (2.15), $c_{\mathrm{eff}}(T) = k_B\theta(T)/(\hbar n^{1/3}h(T))$ (red solid curve). The atomic density of rutile is $n_{\mathrm{rutile}} = 9.569 \times 10^{22}$ /cm^3, cf. Section 5.2. The effective phonon speed $c_{\mathrm{eff}}(T)$ converges to finite limit values at low and high temperature, cf. (3.12) and (3.19). At low temperature, $c_{\mathrm{eff}}(T)$ approaches the constant effective phonon speed of the Debye approximation (depicted as black dashed straight line), cf. (3.25). The constant high-temperature limit of $c_{\mathrm{eff}}(T)$ is not attained below the melting point of 2116 K. For comparison, measured longitudinal/transversal sound velocities in rutile are highly anisotropic and vary between 3.3 km/s and 10.7 km/s [31]. (For interpretation of the references to colour in this figure legend, the reader is referred to the Web version of this article.)

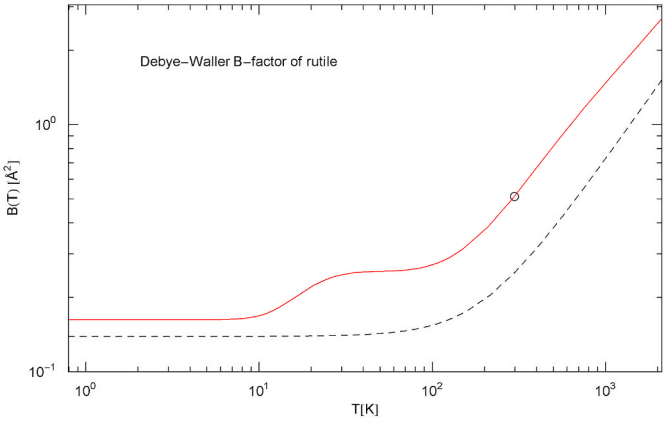

Fig. 6. Mean B-factor of rutile. The red solid curve depicts $B(T)$ in (5.8), depending on the varying Debye temperature $\theta(T)$, cf. Fig. 3, which in turn depends on the zero-point energy U_0, cf. (2.20) and (3.8). At an ambient temperature of 298.15 K, the measured B-factor of rutile is $B_{\mathrm{rutile}} = 0.513$ Å^2 [30] (circle), which is used to determine the zero-point energy, $U_0 = 1.164 \times 10^4$ J/mol, by solving (5.8). Once the zero-point energy is known, the temperature variation of $\theta(T)$ and the spectral cutoff $\Lambda(T)$ is unambiguously determined, cf. Section 5.2. The black dashed curve shows the temperature variation of the B-factor of the Debye approximation, cf. Section 3.4, with constant Debye temperature $\theta = 776.6$ K substituted into (5.8). Evidently, this curve largely deviates from the measured B-factor at 298.15 K. (For interpretation of the references to colour in this figure legend, the reader is referred to the Web version of this article.)

plot of the rutile heat capacity in Fig. 1. Moreover, once the Debye temperature has been obtained from the measured amplitude of the low-temperature heat capacity, this already determines the Debye-Waller $B(T)$ factor, which tends to differ from the measured values (as exemplified by Fig. 6), since there is no free parameter left to adjust this factor. Here, we introduced a temperature-dependent spectral cutoff $\Lambda(T)$ and Debye temperature $\theta(T)$, so that the phonon partition function

still defines an equilibrium system, cf. Section 2, and explained the reconstruction of these functions from measured heat capacity data, cf. Section 3. In this way, we arrived at an equilibrium partition function defining a lattice heat capacity that coincides with the data sets over the full temperature range of the solid phase, cf. Fig. 1.

In general, a partition function with a temperature-dependent Hamiltonian does not define an equilibrium system, since the equilibrium condition $\partial S/\partial U = 1/T$ (necessary to equilibrate with a thermometer system, for instance) is not met [36], but in the case of the phonon partition function (2.1), $\theta(T)$ and $\Lambda(T)$ can be chosen to satisfy this condition, cf. (2.10). The formalism is non-perturbative and can also be used at high pressure.

In Section 4, we studied the heat capacity of rutile. The log-log plots of Fig. 1 depict a least-squares fit to the experimental lattice heat capacity as well as the Debye approximation with constant Debye temperature. The fit function (4.1) is a multiply broken power law with parameters in Table 1, which can be temperature integrated to obtain the entropy variable and the thermal component $U_{\rm therm}(T)$ of the internal energy, cf. Fig. 2. The zero-point internal energy U_0 of rutile was estimated in Section 5.2, from an X-ray diffraction measurement of the Debye-Waller factor.

Once the temperature dependence of the entropy $S(T)$ and internal energy $U(T) = U_{\rm therm}(T) + U_0$ has been quantified by integration of the regressed analytic heat capacity, cf. (2.20), one can calculate the varying Debye temperature $\theta(T)$ and spectral cutoff $\Lambda(T)$ of the partition function as explained in Sections 3.1 and 5. The temperature variation of the Debye temperature of rutile is depicted in Fig. 3, the spectral cutoff in Fig. 4, and the effective phonon speed determining the temperature-dependent dispersion relation $\omega = c_{\rm eff}(T)k$ in the partition function (2.1) is shown in Fig. 5. The temperature variation of the Debye-Waller factor $B(T)$ of rutile is depicted in Fig. 6, from the low-temperature regime up to the melting point, and coincides with the measured value at ambient temperature.

Declaration of competing interest

The author declares that he has no known competing financial interests or personal relationships that could have appeared to influence the work reported in this paper.

Appendix A. Effective phonon Hamiltonian with temperature-dependent dispersion relation

We sketch a derivation of the thermodynamic variables stated in Section 2, based on conventional box quantization. The effective phonon Hamiltonian is defined by an ensemble of one-dimensional harmonic oscillators,

$$H_{\rm eff}(T,n) = \sum_{j,\mathbf{k}} \frac{1}{2}\left(p_{j,\mathbf{k}}^2 + \omega_{j,\mathbf{k}}^2(T,n) q_{j,\mathbf{k}}^2\right), \tag{A.1}$$

where the oscillator frequencies $\omega_{j,\mathbf{k}}(T,n)$ depend on the temperature and atomic density n (of the crystal or amorphous solid) and admit the linear dispersion relation $\omega_{j,\mathbf{k}} = c_j(T,n)k$. The wave vector of the phonons is discretized as $\mathbf{k} = 2\pi\mathbf{n}/L$, $\mathbf{n} \in Z^3$, where L is the box size, and k denotes the wavenumber. The index $j = 1,2,3$ labels the longitudinal and the two transversal polarization degrees. The position and momentum operators satisfy the commutation relation $[q_{j,\mathbf{k}}, p_{j',\mathbf{k}'}] = \mathrm{i}\delta_{jj'}\delta_{\mathbf{k}\mathbf{k}'}$. By introducing the rescaled variables $Q_{j,\mathbf{k}} = \sqrt{\omega_{j,\mathbf{k}}}q_{j,\mathbf{k}}$ and $P_{j,\mathbf{k}} = p_{j,\mathbf{k}}/\sqrt{\omega_{j,\mathbf{k}}}$ as well as bosonic annihilation and creation operators, $a_{j,\mathbf{k}} = \left(Q_{j,\mathbf{k}} + \mathrm{i}P_{j,\mathbf{k}}\right)/\sqrt{2}$ and $a_{j,\mathbf{k}}^\dagger = \left(Q_{j,\mathbf{k}} - \mathrm{i}P_{j,\mathbf{k}}\right)/\sqrt{2}$, the Hamiltonian (A.1) can be written as

$$H_{\rm eff}(T,n) = \sum_{j,\mathbf{k}} \frac{1}{2}\omega_{j,\mathbf{k}}\left(P_{j,\mathbf{k}}^2 + Q_{j,\mathbf{k}}^2\right) = \sum_{j,\mathbf{k}} \omega_{j,\mathbf{k}}(T,n)\left(N_{j,\mathbf{k}} + \frac{1}{2}\right). \tag{A.2}$$

The $N_{j,\mathbf{k}} = a_{j,\mathbf{k}}^\dagger a_{j,\mathbf{k}}$ are commuting hermitian particle number operators, and a multi-index notation $i = (j,\mathbf{k})$ will be used as shortcut for the summation indices. The a_i and their adjoints satisfy the commutation relations $[a_i, a_n^\dagger] = \delta_{in}$.

The operators a_i and $a_i^\dagger$ will be used in occupation number representation, with normalized basis vectors $|n_1,\cdots,n_i,\cdots,n_\infty\rangle$ (shortcut $|n\rangle$, e.g., $|0\rangle$ for the vacuum state). The occupation numbers n_i are non-negative integers indicating the number of particles in state i. A scalar product is defined by $\langle n|n'\rangle = \delta_{n_1,n_1'}\ldots\delta_{n_\infty,n_\infty'}$. The representation of the a_i and $a_i^\dagger$ then reads

$$\begin{aligned} a_i|n_1,\cdots,n_i,\cdots,n_\infty\rangle &= \sqrt{n_i}|n_1,\cdots,n_i-1,\cdots,n_\infty\rangle,\\ a_i^\dagger|n_1,\cdots,n_i,\cdots,n_\infty\rangle &= \sqrt{n_i+1}|n_1,\cdots,n_i+1,\cdots,n_\infty\rangle, \end{aligned} \tag{A.3}$$

and $a_i|n\rangle = 0$ (zero-vector) if $n_i = 0$. Hence, $\langle a_i^\dagger n|n'\rangle = \langle n|a_i n'\rangle$. The particle number operators $N_i = a_i^\dagger a_i$ are hermitian, commute, and are diagonal in this representation, $N_i|n\rangle = n_i|n\rangle$.

The density operator reads $\widehat{\rho} = \exp(-H_{\rm eff}(T,n)/T)$, the partition function is defined by the trace $Z = \mathrm{Tr}[\widehat{\rho}]$, and the total internal energy is obtained as expectation value $U = \langle H_{\rm eff}\rangle$, $\langle H_{\rm eff}\rangle = \mathrm{Tr}[H_{\rm eff}\widehat{\rho}]/Z$. To evaluate the expectation value of an operator of type $G(T,n) = \sum_{j,\mathbf{k}} g_{j,\mathbf{k}}(T,n)(N_{j,\mathbf{k}} + 1/2)$, where $g_{j,\mathbf{k}}$ is an arbitrary function of polarization index j and wave vector $\mathbf{k}$ and other parameters such as temperature and atomic density, we consider $Z_\varepsilon = \mathrm{Tr}[\widehat{\rho}_\varepsilon]$ with $\widehat{\rho}_\varepsilon = \exp[-H_{\rm eff}(T,n)/T - \varepsilon G(T,n)]$. Here, ε is a dimensionless parameter put to zero after differentiation, so that $\langle G\rangle = -(\log Z_\varepsilon)_{,\varepsilon} = \mathrm{Tr}[G\widehat{\rho}]/Z$. Employing the above stated occupation number representation, $\log Z_\varepsilon$ can easily be evaluated. We write

$$H_{\rm eff}/T + \varepsilon G = \sum_{j,\mathbf{k}} f_{j,\mathbf{k}}\left(N_{j,\mathbf{k}} + \frac{1}{2}\right), \quad f_{j,\mathbf{k}} := \frac{\omega_{j,\mathbf{k}}(T,n)}{T} + \varepsilon g_{j,\mathbf{k}}(T,n), \tag{A.4}$$

and find, in multi-index notation $i = (j,\mathbf{k})$,

$$Z_\varepsilon = \sum_{n_1,\cdots,n_\infty=0}^{\infty} \exp(-\sum_{i=1}^{\infty} f_i(n_i+\frac{1}{2})) = \sum_{n_1,\cdots,n_\infty=0}^{\infty} \prod_{i=1}^{\infty} \exp(-f_i(n_i+\frac{1}{2}))$$
$$= \prod_{i=1}^{\infty}\sum_{n_i=0}^{\infty} \mathrm{e}^{-f_i(n_i+1/2)} = \prod_{i=1}^{\infty} \mathrm{e}^{-f_i/2}\sum_{n_i=0}^{\infty}\mathrm{e}^{-f_i n_i} = \prod_{i=1}^{\infty}\frac{\mathrm{e}^{-f_i/2}}{1-\mathrm{e}^{-f_i}}. \tag{A.5}$$

Thus,

$$\log Z_\varepsilon = \sum_{i=1}^{\infty}\log\frac{\mathrm{e}^{-f_i/2}}{1-\mathrm{e}^{-f_i}} = -\sum_{j,\mathbf{k}}\big(f_{j,\mathbf{k}}/2+\log\big(1-\mathrm{e}^{-f_{j,\mathbf{k}}}\big)\big), \tag{A.6}$$

and, by substitution of $f_{j,\mathbf{k}}$ (defined in (A.4)),

$$\langle G\rangle = -(\log Z_\varepsilon)_{,\varepsilon} = \sum_{j,\mathbf{k}} g_{j,\mathbf{k}}\left(\frac{1}{\mathrm{e}^{\omega_{j,\mathbf{k}}/T}-1}+\frac{1}{2}\right). \tag{A.7}$$

The continuum limit is performed by replacing $\sum_{\mathbf{k}}\to(L^3/(2\pi)^3)\int \mathrm{d}\mathbf{k}$, so that

$$\log Z_\varepsilon = -\frac{L^3}{(2\pi)^3}\sum_j\int\left(\log\big(1-\mathrm{e}^{-f_{j,\mathbf{k}}}\big)+\frac{1}{2}f_{j,\mathbf{k}}\right)\mathrm{d}\mathbf{k}, \tag{A.8}$$

$$\langle G\rangle = \frac{L^3}{(2\pi)^3}\sum_j\int g_{j,\mathbf{k}}(T,n)\left(\frac{1}{\mathrm{e}^{\omega_{j,\mathbf{k}}(T,n)/T}-1}+\frac{1}{2}\right)\mathrm{d}\mathbf{k}. \tag{A.9}$$

The expression in parentheses in (A.9) is just $(1/2)\coth(\omega_{j,\mathbf{k}}/(2T))$.

To obtain the internal energy $U=\langle H_{\mathrm{eff}}\rangle$, we put $g_{j,\mathbf{k}}=\omega_{j,\mathbf{k}}=c_j(T,n)k$ in (A.9) (which means $H_{\mathrm{eff}}=\sum_{j,\mathbf{k}}\omega_{j,\mathbf{k}}(T,n)(N_{j,\mathbf{k}}+1/2)$, see after (A.3)) and find

$$\frac{\langle H_{\mathrm{eff}}\rangle}{L^3} = \frac{4\pi}{(2\pi)^3}\sum_j c_j(T,n)\int\left(\frac{1}{\mathrm{e}^{c_j(T,n)k/T}-1}+\frac{1}{2}\right)k^3\mathrm{d}k. \tag{A.10}$$

Analogously, the effective phonon number $\langle N_{\mathrm{ph}}\rangle$, cf. (2.14), is obtained by putting $g_{j,\mathbf{k}}=1$ in (A.9), which means $N_{\mathrm{ph}}=\sum_{j,\mathbf{k}}(N_{j,\mathbf{k}}+1/2)$ and

$$\frac{\langle N_{\mathrm{ph}}\rangle}{L^3} = \frac{4\pi}{(2\pi)^3}\sum_j\int\left(\frac{1}{\mathrm{e}^{c_j(T,n)k/T}-1}+\frac{1}{2}\right)k^2\mathrm{d}k. \tag{A.11}$$

The average $\langle N_{\mathrm{ph}}\rangle$ is not to be confused with the effective oscillator number, $N_{\mathrm{oscil}}=\sum_{j,\mathbf{k}}1$, which, in the thermodynamic limit, reads $N_{\mathrm{oscil}}/L^3 = (4\pi/(2\pi)^3)\sum_j\int k^2\mathrm{d}k$, cf. after (A.7) and (2.14).

The entropy $\langle S\rangle=-\mathrm{Tr}[\widehat{\rho}_S\log\widehat{\rho}_S]$ is defined by the normalized density operator $\widehat{\rho}_S=\widehat{\rho}/Z$, $\widehat{\rho}=\exp(-H_{\mathrm{eff}}(T,n)/T)$, see after (A.3), so that $\mathrm{Tr}[\widehat{\rho}_S]=1$ and $\langle S\rangle=\log Z+\langle H_{\mathrm{eff}}\rangle/T$. The thermodynamic limit of $\log Z$ is stated in (A.8), with $\varepsilon=0$ and $f_{j,\mathbf{k}}=\omega_{j,\mathbf{k}}(T,n)/T$, cf. (A.4),

$$\log Z = -\frac{4\pi L^3}{(2\pi)^3}\sum_j\int\left(\log\big(1-\mathrm{e}^{-c_j(T,n)k/T}\big)+\frac{1}{2}\frac{c_j(T,n)k}{T}\right)k^2\mathrm{d}k. \tag{A.12}$$

In Section 2, we specify the integration range of the wavenumber integration $\mathrm{d}k$ by introducing a temperature-dependent upper integration boundary $\Lambda(T,n)$ in (A.8)-(A.12). This spectral cutoff can be chosen so that $\log Z$ becomes the partition function of an equilibrium system, despite the explicit temperature dependence of the dispersion relation $\omega_{j,\mathbf{k}}=c_j(T,n)k$, cf. Section 2.2. We use the same effective phonon speed for the longitudinal and transversal polarizations, so that the dispersion relation simplifies to $\omega=c_{\mathrm{eff}}(T,n)k$. The partition function (A.12) then reads as stated in (2.1).

Finally we indicate a derivation of the mean-squared atomic vibrations $\langle u_Q^2\rangle$ in (5.1) and (5.3). The expectation values of the squared momentum and position variables (with regard to the n-th energy eigenstate) of a one-dimensional harmonic oscillator read $\langle p^2\rangle=m\omega_n$ and $\langle q^2\rangle=\omega_n/(m\omega^2)$, where $\omega_n=(n+1/2)\omega$ are the energy eigenvalues. (The ground state energy $\omega/2$ is related to the coupling constant $\widehat{k}$ of the harmonic potential by $\omega^2=\widehat{k}/m$, and m is the oscillator mass.) Thus the kinetic energy $\langle p^2\rangle/(2m)$ equals the potential energy $m\omega^2\langle q^2\rangle/2$, so that the total energy of an oscillator can be expressed as $\langle H\rangle=m\omega^2\langle q^2\rangle$. The spectral energy density of the atomic oscillators constituting the solid is $\rho_E(\omega)=n_{\mathrm{oscil}}m\omega^2\langle q^2\rangle$, with oscillator density $n_{\mathrm{oscil}}=N_{\mathrm{oscil}}/V$, cf. after (2.14), so that $\langle q^2\rangle=\rho_E(\omega)/\big(n_{\mathrm{oscil}}m\omega^2\big)$. On the other hand, we may use $\omega=c_{\mathrm{eff}}(T,n)k$ as integration variable in energy density (2.7),

$$u=\int_0^{\theta(T)}\rho_E(\omega)\mathrm{d}\omega,\quad \rho_E(\omega)=\frac{4\pi\sigma}{(2\pi)^3c_{\mathrm{eff}}^3(T)}\left(\frac{1}{\mathrm{e}^{\omega/T}-1}+\frac{1}{2}\right)\omega^3, \tag{A.13}$$

so that the frequency-integrated $\langle q^2\rangle$ at finite temperature reads

$$\langle u_Q^2\rangle=\int_0^{\theta(T)}\langle q^2\rangle\mathrm{d}\omega=\frac{4\pi\sigma}{(2\pi)^3mc_{\mathrm{eff}}^3(T)n_{\mathrm{oscil}}(T)}\int_0^{\theta(T)}\left(\frac{1}{\mathrm{e}^{\omega/T}-1}+\frac{1}{2}\right)\omega\mathrm{d}\omega, \tag{A.14}$$

which coincides with $\langle u_Q^2\rangle$ in (5.3), if we use $c_{\rm eff}=\theta(T)/\Lambda(T)$ and $n_{\rm oscil}=(4\pi\sigma/(2\pi)^3)\Lambda^3(T)/3$, cf. after (2.14), and restore the units.

References

[1] W.T. Berg, J.A. Morrison, Proc. Roy. Soc. (London) A 242 (1957) 467.
[2] D.M. Hoat, J.F. Rivas Silva, A. Méndez Blas, Physica B 545 (2018) 55.
[3] B.-L. Yan, H. Qin, Z.-K. He, Y. Wei, K. Chang, B.-L. Guo, B. Tang, D.-H. Fan, Q.-J. Liu, Physica B 546 (2018) 1.
[4] D.M. Hoat, Physica B 558 (2019) 109.
[5] M. Peng, H. Shou, Y. Cao, Physica B 561 (2019) 29.
[6] Z. Kong, Y. Duan, M. Peng, D. Qu, L. Bao, Physica B 573 (2019) 13.
[7] D.A.H. Hanaor, C.C. Sorrell, J. Mater. Sci. 46 (2011) 855.
[8] G. Meinhold, Earth Sci. Rev. 102 (2010) 1.
[9] K.T. Matsumoto, N. Morioka, K. Hiraoka, Physica B 533 (2018) 90.
[10] A.A. Musari, D.P. Joubert, G.A. Adebayo, Physica B 552 (2019) 159.
[11] A. Bakar, A. Afaq, M.F. Khan, N. ul Aarifeen, M.I. Jamil, M. Asif, Physica B 576 (2020), 411715.
[12] X.D. Li, K. Li, C.H. Wei, W.D. Han, N.G. Zhou, Physica B 538 (2018) 54.
[13] Y. Amakai, S. Murayama, N. Momono, H. Takano, T. Kuwai, Physica B 536 (2018) 173.
[14] S.A. Sofi, D.C. Gupta, Physica B 577 (2020), 411792.
[15] P. Amiri, H. Salehi, Y.L. Motlagh, Physica B 578 (2020), 411761.
[16] A.N. Filanovich, A.A. Povzner, Physica B 527 (2017) 16.
[17] A.N. Filanovich, A.A. Povzner, Physica B 575 (2019), 411693.
[18] K.V. Khishchenko, V.E. Fortov, I.V. Lomonosov, Int. J. Thermophys. 26 (2005) 479.
[19] E. Eser, H. Koç, Physica B 492 (2016) 7.
[20] S.Sh. Rekhviashvili, Kh. L. Kunizhev, High Temp. 55 (2017) 312.
[21] M. Abramowitz, I.A. Stegun, Handbook of Mathematical Functions, Dover Publ., New York, 1972.
[22] T. Mitsuhashi, Y. Takahashi, J. Ceram. Ass. Japan 88 (1980) 305.
[23] D. de Ligny, P. Richet, E.F. Westrum Jr., J. Roux, Phys. Chem. Miner. 29 (2002) 267.
[24] J.S. Dugdale, J.A. Morrison, D. Patterson, Proc. Roy. Soc. Lond. A 224 (1954) 228.
[25] T.R. Sandin, P.H. Keesom, Phys. Rev. 177 (1969) 1370.
[26] R. Tomaschitz, Physica A 483 (2017) 438.
[27] R. Tomaschitz, Physica A 541 (2020), 123188.
[28] R. Tomaschitz, Appl. Phys. A 126 (2020) 102.
[29] R.W. James, The Optical Principles of the Diffraction of X-Rays, Bell, London, 1967.
[30] J.-S. Jeon, B.-H. Kim, C.-I. Park, S.-Y. Seo, C. Kwak, S.-H. Kim, S.-W. Han, Jpn. J. Appl. Phys. 49 (2010), 031105.
[31] M.H. Manghnani, E.S. Fisher, W.S. Brower Jr., J. Phys. Chem. Solids 33 (1972) 2149.
[32] N.M. Butt, J. Bashir, P.T.M. Willis, G. Heger, Acta Crystallogr. A 44 (1988) 396.
[33] N.M. Butt, J. Bashir, M.N. Khan, Acta Crystallogr. A 49 (1993) 171.
[34] R.C.G. Killean, E.J. Lisher, J. Phys. F Met. Phys. 5 (1975) 1107.
[35] C.K. Shepard, J.G. Mullen, G. Schupp, Phys. Rev. B 61 (2000) 8622.
[36] R. Tomaschitz, Fluid Phase Equilib. 496 (2019) 80.